J Appl Electrochem (2012) 42:443–453
DOI 10.1007/s10800-012-0418-0

ORIGINAL PAPER

Investigation of design parameter effects on high current performance of lithium-ion cells with $LiFePO_4$/graphite electrodes

Seungho Yu · Youngmin Chung · Min Seob Song · Jin Hyun Nam · Won Il Cho

Received: 16 February 2012 / Accepted: 12 April 2012 / Published online: 28 April 2012

Abstract Electrode design is an essential task for successful development of lithium-ion batteries. Provided that the same materials are given, proper dimensioning of the electrodes and balanced composition of the materials in them can maximize the cell performance, such as the discharge capacity. However, many electrode design parameters have conflicting effects on the performance, and thus careful optimization of these parameters is required. This study experimentally investigated the effects of several electrode design parameters on the performance of lithium ion cells with a $LiFePO_4$ cathode and a natural graphite anode, focusing on their high current operations. The conflicting effects of the conductor ratio (the weight fraction of electronic particle additives), electrode thickness, and electrode density (porosity) on the cell capacity were studied. In addition, a detailed one-dimensional electrochemical model was also used to simulate the observed performance characteristics and to identify their underlying mechanisms limiting the performance. Based on the experimental and numerical results, the optimal ranges for the electrode design parameters were discussed to achieve better performance of the $LiFePO_4$/graphite batteries.

S. Yu · Y. Chung · M. S. Song · W. I. Cho (✉)
Center for Energy Convergence, Korea Institute of Science and Technology, 39-1 Hawolgok-dong, Seongbuk-gu, Seoul 136-791, Republic of Korea
e-mail: wonic@kist.re.kr

J. H. Nam (✉)
School of Mechanical and Automotive Engineering, Daegu University, Gyungsan 712-714, Republic of Korea
e-mail: jinhnam@gmail.com

Keywords Lithium-ion battery · $LiFePO_4$ · Battery design parameter · Electrode thickness · Active material density · Electrochemical modeling

List of symbols

Variables

a_i	Specific surface area of electrode i (i = n, p) (m^{-1})
c	Electrolyte concentration (mol m^{-3})
$c_{s,i}$	Concentration of lithium in the AM particle of electrode i (i = n, p) (mol m^{-3})
D	Electrolyte diffusion coefficient (m^2 s^{-1})
$D_{s,i}$	Lithium-ion diffusion coefficient in the AM particle of electrode i (i = n, p) (m^2 s^{-1})
F	Faraday's constant (C mol^{-1})
I	Applied current density (A cm^{-2})
j_i	Wall flux of Li ion on the intercalation particle of electrode i (i = n, p) (mol m^{-2} s^{-1})
k_i	Reaction-rate constant of electrode i (i = n, p) [mol (mol m^{-3})$^{-1.5}$]
l_i	Thickness of electrode i (i = n, s, p) (m)
n	Negative electrode
p	Positive electrode
r	Radial coordinate (m)
R	Universal gas constant [J (mol K)$^{-1}$]
R_i	Radius of the AM particle of electrode i (i = n, p) (m)
s	Separator
t_+	Li ion transference number in the electrolyte
T	Absolute temperature (K)
U_i	Open-circuit potential of electrode i (i = n, p) (V)
x	Spatial coordinate (m)

Greek letters

ε_i Porosity of electrode i (i = n, s, p)
$\varepsilon_{f,i}$ Volume fraction of fillers of electrode i (i = n, p)
$\varepsilon_{p,i}$ Volume fraction of polymer of electrode i (i = n, p)
$\kappa_{eff,i}$ Effective ionic conductivity of the electrolyte in region i (i = n, s, p) (S m^{-1})
σ_i Electronic conductivity of the solid phase of electrode i (i = n, p) (S m^{-1})
$\sigma_{eff,i}$ Effective electronic conductivity of the solid phase of electrode i (i = n, p) (S m^{-1})
Φ_1 Solid-phase potential (V)
Φ_2 Electrolyte-phase potential (V)

1 Introduction

Lithium iron phosphate ($LiFePO_4$) has received much research attention as a promising active material (AM) for rechargeable lithium-ion batteries, primarily due to its lower cost, better safety, lower toxicity, and longer cycle life, compared to other AMs developed before. Among various application fields, the automotive application for powering electric vehicles (EVs) and hybrid electric vehicles (HEVs) is expected to be most benefited by the development of the lithium-ion batteries employing the $LiFePO_4$ electrode. High current rate, long cycle performance and good thermal stability of $LiFePO_4$ provide ideal characteristics for automotive batteries that require higher power demand and better safety.

Experimental researches on $LiFePO_4$ were initially focused on enhancing the discharge capacity by improving the electronic conductivity or ionic diffusivity in the solid state. Thus, the carbon coating [1–4], the metallic element doping [5–7], and the size reduction [8–10] of $LiFePO_4$ particles have been studied to improve the electrochemical performance. Besides these particle-scale researches, many recent studies were also focused on improving the electronic and ionic transport by the electrode-scale modification, aiming to obtain the optimized electrode microstructures. These optimization studies have generally sought to determine the optimal ranges for the electrode design parameters including the AM particle size, electrode thickness, AM density (porosity), and conductor ratio (the weight fraction of electronic particle additives) [11–14]. However, the electrode optimization is a difficult task because of the abundance of the electrode design parameters that need to be tested as well as their complex interplay influencing the performance [15].

Numerical modeling can help the optimization procedure by predicting the effects of the electrode design parameters on the performance of lithium-ion batteries as well as by clarifying the underlying mechanisms that limit the battery performance. The mathematical models developed by Newman group [16–19] have been widely utilized for numerical simulation of various lithium-ion battery systems. Srinivasan and Newman [20, 21] proposed a mathematical model for lithium-ion batteries based on a $LiFePO_4$ cathode and a natural graphite anode and investigated the effects of the electrode thickness and porosity to maximize the specific energy. The shrinking core model for the solid-phase diffusion in $LiFePO_4$ particles proposed by Srinivasan and Newman [20, 21] was found to show a good agreement between the experimental and numerical results. A more accurate model accounting for the phase transition with anisotropic diffusion in $LiFePO_4$ particles was also reported recently [22–24]; however, this model is difficult to be used for the full cell simulation of lithium-ion batteries.

In this study, the design parameters for a $LiFePO_4$ cathode were investigated through systematic experiments using coin cells as well as numerical simulations. The electrode design parameters including the conductor ratio, electrode thickness, and AM density of the $LiFePO_4$ cathode were considered aiming to achieve high discharge capacity at high current rates. In general, carbon conductor is used to improve the electronic conductivity of the $LiFePO_4$ cathode, but this may reduce the volumetric energy density and/or accelerate the decomposition of electrolyte solvent [25, 26]. Thus, it is important to optimize the conductor ratio to obtain better performance of lithium-ion batteries. The effects of the conductor ratio on the performance of the $LiFePO_4$ cathode were examined first through half cell tests with a lithium metal anode. Full cell tests were also performed using coin cells with a $LiFePO_4$ cathode and a graphite anode to investigate the coulombic efficiency at various P/N mass ratios and the capacity variation at low current rates. Based on these experimental results, the conductor ratio and the P/N mass ratio were determined for subsequent experimental investigations.

The effects of the electrode thickness and AM density on the discharge capacity were then investigated. Thick and dense electrodes generally increase the energy density, but they can reduce the discharge capacity at high current operations primarily due to the transport-related limitations [20]. Thus, it is also important to identify the critical values for the electrode thickness or density, above which the transport loss becomes significantly larger than acceptable. Tests were performed using coin cells with a $LiFePO_4$ cathode and a graphite anode, by varying the electrode thickness and AM density. In addition, a one-dimensional (1D) electrochemical model for lithium-ion batteries was also used to analyze the observed effects on the cell performance with the $LiFePO_4$/graphite electrodes. Based on the experimental and numerical results, the optimal ranges for the electrode thickness and AM density were discussed to achieve higher discharge capacity and efficiency at high current operations.

2 Methods

2.1 Experimental

A $LiFePO_4$ AM was supplied from a company (SK Innovation Co., Korea). A slurry was made by mixing the $LiFePO_4$ powder with polyvinylidene fluoride (PVDF) binder and acetylene black (AB) conductor powder in N-methyl pyrrolidone (NMP) solvent. To study the effects of conductor ratio, the weight percent (wt%) of AB in the slurry was varied from 2 to 15 wt%. The amount of PVDF binder was controlled to be constant at 6 wt%. Then, the slurry was coated onto an Al foil to form an electrode layer (about 60 μm thickness) and dried in an oven at 80 °C for 4 h. The amount of NMP was found to be enough to facilitate the homogeneous mixing of AM and AB.

After the casting and drying, the electrode was compressed in a rolling machine at 120 °C, and this reduced the electrode thickness by about 30 % toward the target thickness for the half cell tests (from around 60 μm to around 40 μm). Then, the compressed electrode was further dried in a vacuum oven at 80 °C for 12 h. The half cell tests were performed using lithium metal as an anode. A $LiFePO_4$ cathode and a lithium metal anode were placed in a standard coin cell construction (2032 type) and 1 M $LiPF_6$ in an ethylene carbonate/dimethyl carbonate/ethylmethyl carbonate solution was added as an electrolyte. The electrochemical behaviors of these half cells were measured for several galvanostatic charge/discharge cycles using a battery cycler (Maccor 4000, Maccor Inc., USA). The charge/discharge current rate was varied as 0.5, 1, 5, 10, and 20 C with a cut-off voltage range of 2.5–4.0 V.

The effects of the conductor ratio on the cell performance were further investigated through full cell tests with a $LiFePO_4$ cathode and a graphite anode. To construct the full cell structure, $LiFePO_4$, and graphite (SK Innovation Co., Korea) were mixed with PVDF and AB in an NMP solvent, and then each slurry was coated onto an Al foil or a Cu foil, respectively, to form a cathode or an anode. As before, the amount of AB powder added to the $LiFePO_4$ slurry was between 4 and 15 wt%. The mixing ratio was maintained constant as 0 wt% for AB and 5 wt% for PVDF in the graphite anode.

After the conductor ratio tests, the effects of the electrode thickness and AM density were investigated to determine the optimal ranges for these parameters. The thickness of the $LiFePO_4$ cathode was controlled by varying the amount of NMP added to the slurry and also the height of the doctor blade used to form an electrode layer. The thickness of the graphite anode was determined proportional to the capacity (or the thickness) of the $LiFePO_4$ cathode to be combined. After the compaction by about 30–45 %, both electrodes were dried in a vacuum oven at 80 °C for 12 h. The thickness of the $LiFePO_4$ cathode was varied as 55–125 μm, and the AM density were about 1.93–2.30 g cm^{-3}. These tests were also performed galvanostatically, similar to the previous cell tests, with a cut-off voltage range of 2.5–4.0 V. The charge/discharge current rates from 0.2 to 5 C were considered.

2.2 Numerical

A numerical code was used in this study to simulate the discharge curves that were obtained from the experimental tests with the $LiFePO_4$/graphite cells. Based on the mathematical model of Newman group, this code can consider the electrochemical and transport processes in the 1D lithium ion battery structure consisting of a positive electrode, a separator, and a negative electrode. The mass transport inside spherical AM particles was also coupled with the electrode-scale processess. The governing equations for the lithium ion battery simulation are presented in Table 1 for each calculation region. As indicated in Table 1, this numerical code solves the electrolyte concentration, c, the electrolyte potential, Φ_2, the solid concentration, c_s, and the solid potential, Φ_1, as the main variables, along with the local current density, j_i, due to electrochemical reactions. The finite difference method with implicit time marching was used to discretize the governing equations. The relevant boundary conditions are also provided in Table 2.

Table 3 summarizes the correlations for the battery simulation, including the effective solid-phase conductivity, $\sigma_{\text{eff},i}$, the effective electrolyte-phase conductivity, $k_{\text{eff},i}$, the effective electrolyte-phase diffusivity, $D_{\text{eff},i}$, and the active surface area per unit volume in the electrodes. The equilibrium potentials for the positive and negative electrodes, U_p and U_n, in Table 3 were determined based on the experimentally measured discharge curve at the current rate of 0.05 C. The physical parameters required for the simulations are summarized in Tables 4 and 5. Note that these parameters are chosen from actual measurement or from other references.

3 Results and discussion

3.1 Conductor ratio test

The effect of conductor ratio in the $LiFePO_4$ electrode was examined first, using half cells with lithium metal as a counter electrode. The thickness of the $LiFePO_4$ electrode was controlled to be about 40 μm. For such thin electrodes, the voltage loss due to ohmic and ionic diffusion resistances is generally expected to be small for ordinary discharge operations at below 1 C rate. Figure 1 shows the discharge

Table 1 Governing equations for the battery simulations [16]

Region	Governing equations
Electrode	
Solid potential (Φ_1)	$\sigma_{\text{eff},i}\frac{\partial^2\Phi_1}{\partial x^2} = a_i F j_i$
Electrolyte potential (Φ_2)	$-\sigma_{\text{eff},i}\frac{\partial\Phi_1}{\partial x} - k_{\text{eff},i}\frac{\partial\Phi_2}{\partial x} + \frac{2k_{\text{eff},i}\text{RT}}{F}(1-t_+)\frac{\partial \ln c}{\partial x} = I$
Electrolyte concentration (c)	$\varepsilon_i\frac{\partial c}{\partial t} = D_{\text{eff},i}\frac{\partial^2 c}{\partial x^2} + a_i(1-t_+)j_i$
Solid concentration (c_s)	$\frac{\partial c_s}{\partial t} = \frac{D_{s,i}}{r^2}\frac{\partial}{\partial r}\left(r^2\frac{\partial c_s}{\partial r}\right)$
Local current density (j_i)	$j_i = 2k_i\left(c_{s,\max,i} - c_{s,i}\big\vert_{r=R_i}\right)^{0.5} c_{s,i}\big\vert_{r=R_i}^{0.5} c^{0.5} \times \sinh\left[\frac{0.5F}{\text{RT}}(\Phi_1 - \Phi_2 - U_i)\right]$
Separator	
Electrolyte concentration (c)	$\varepsilon_i\frac{\partial c}{\partial t} = D_{\text{eff},i}\frac{\partial^2 c}{\partial x^2}$
Electrolyte potential (Φ_2)	$-k_{\text{eff},i}\frac{\partial^2\Phi_2}{\partial x^2} + \frac{2k_{\text{eff},i}\text{RT}}{F}(1-t_+)\frac{\partial \ln c}{\partial x} = I$

$i = n$ (negative), p (positive), s (separator)

Table 2 Boundary conditions for the battery simulations [16]

Boundary conditions	Electrode–separator interface	Electrode–current collector interface
Solid potential (Φ_1)	$-\sigma_{\text{eff},i}\frac{\partial\Phi_1}{\partial x} = 0$	$-\sigma_{\text{eff},i}\frac{\partial\Phi_1}{\partial x} = I$
Electrolyte potential (Φ_2)	Continuous	$-k_{\text{eff},i}\frac{\partial\Phi_2}{\partial x} = 0$
Concentration (c)	Continuous	$-D_{\text{eff},i}\frac{\partial c}{\partial x} = 0$
Solid concentration (c_s)	$\frac{\partial c_s}{\partial r}\big\vert_{r=0} = 0, \quad j_i = -D_{s,i}\frac{\partial c_s}{\partial r}\big\vert_{r=R_i}$	

Table 3 Correlations used in the battery simulations

$\sigma_{\text{eff},i} = \sigma_i(1-\varepsilon_i-\varepsilon_{f,i}-\varepsilon_{p,i}), \quad i = n,p$

$k_{\text{eff},i} = \varepsilon_i^{1.5}(0.0911 + 1.9101c - 1.052c^2 + 0.1554c^3), \quad i = \text{n, s, p}$

$D_{\text{eff},i} = D_i\varepsilon_i^{1.5}, \quad i = \text{n, s, p}$

$a_i = \frac{3}{R_i}(1-\varepsilon_i-\varepsilon_{f,i}-\varepsilon_{p,i}), \quad i = \text{n, p}$

$U_n = 0.72 + 0.055x + 0.083x^{0.5} - 0.017x^{-1} + 0.0025x^{-2.2} + 0.25\exp(0.9-15x) - 0.78\exp(0.45x-0.4), \quad x = c_{s,n}\,c_{s,n,\max}^{-1}$

$U_p = 3.42 - \exp(-90(0.955-x)^{1.05}) + 0.7\tan^{-1}(90(0.93-x)) + 0.71\tan^{-1}(90(x-1.05)), \quad x = c_{s,p}\,c_{s,p,\max}^{-1}$

capacity (per AM mass) of the $LiFePO_4$ half cell with respect to conductor ratio for the cut-off voltage of 2.5 V. Recall that the AB ratio in the electrode was increased from 2 to 15 wt% while the binder ratio was maintained at 6 wt%. Figure 1 indicates that the discharge capacity of the $LiFePO_4$ electrode remains relatively constant when the conductor ratio becomes larger than 4 wt%. However, the half cell tests cannot properly consider the voltage loss due to ionic diffusion limitation in actual lithium ion batteries, which may be important especially for large electrode thickness and high AM density (low porosity).

Figure 2 presents the SEM images of the $LiFePO_4$ electrodes corresponding to the added conductive AB ratio of 2, 8, and 15 wt%. These images clearly show the change in the electrode microstructure according to the variation in conductor ratio. With increase in conductor ratio, more AB particles (15 nm mean radius) come to reside in the pores between AM particles (150 nm mean radius), thereby forming efficient electronic conduction pathways. Thus, the higher electrode conductivity with higher conductor ratio is easily understood. However, Fig. 2b, c indicates that excess AB in the $LiFePO_4$ electrode may reduce the volumetric energy density. The solid-phase conductivity of the electrode without conductor additives was relatively high around 0.47 S m^{-1} (measured by a four-point probe technique) due to the carbon coating of $LiFePO_4$ particles. In fact, the electrical conductivity of the $LiFePO_4$ electrode was found to reach 9.9 S m^{-1} at the conductor ratio of 5 wt%, which is believed to be enough for good electrical conduction in the electrode. Thus, adding proper amount of AB is important to increase the energy density of electrodes with sufficiently good electron conduction.

Table 4 Physical parameters used in the battery simulations

Parameter	Graphite	$LiFePO_4$
Radius of AM particles[a]	10 μm	150 nm
Diffusion coefficient[b] ($m^2\ s^{-1}$)	2.0×10^{-14}	4.0×10^{-18}
Reaction rate constant[b] (mol $s^{-1}\ m^{-2}$) [(mol m^{-3})$^{-1.5}$]	5×10^{-11}	3.5×10^{-13}
Conductivity[a] (S m^{-1})	100	11
Initial SOC	0.9	0.1
Initial concentration (mol m^{-3})	1,000	
Transport number	0.363	
Thickness of separator (μm)	25	
Separator porosity	0.55	
Faraday's constant (C mol^{-1})	96487	
Temperature (K)	298.15	
Universal gas constant (J $mol^{-1}K^{-1}$)	8.314	

[a] Measured values

[b] Fitted values

Table 5 Electrode parameters used in the battery simulations

Electrode	Porosity (%)	AM (vol%)	AB (vol%)	PVDF (vol%)	AM density (g cm^{-3})	Theoretical capacity (mAh cm^{-2}) @ 100 μm
Positive electrode	31.0	56.76	5.822	6.414	2.05	3.474
	27.4	59.73	6.126	6.749	2.15	3.655
Negative electrode	34	61.95	0	4.05	1.40	5.180

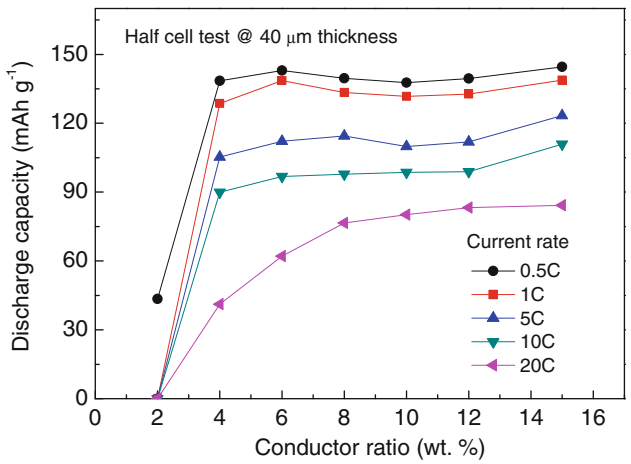

Fig. 1 The discharge capacity of the $LiFePO_4$ half cells (40 μm electrode thickness) at various conductor ratios

The ratio of positive electrode capacity to negative electrode capacity (P/N ratio) is an important design parameter that controls the first-cycle irreversible capacity loss of a lithium-ion battery. Thus, the coulombic efficiency at various P/N ratios was investigated using lithium-ion full cells consisting of a $LiFePO_4$ cathode and a graphite anode. The results are shown in Fig. 3 for the AB ratio of 4, 8, 12, and 15 wt% added to the $LiFePO_4$ electrode. Figure 3 indicates that the proper P/N mass ratio is about 2.0–2.2, and at this P/N ratio the first-cycle capacity loss becomes less than 15 % when measured at 0.1 C current rate. The first-cycle charge and discharge capacities for the P/N mass ratio of 2.0 are also presented in Fig. 4, where the first-cycle capacities are observed to increase proportional to the mass of $LiFePO_4$ material. The charge capacity per AM mass shows a nearly theoretical value while the discharge capacity shows 15 % capacity loss.

Based on these results, the AB ratio of around 5 wt% was chosen as the proper range, considering both the electrical conductivity and the volumetric energy density. In addition, the P/N mass ratio of about 2.0 was also chosen as the suitable range for $LiFePO_4$/graphite lithium ion batteries to obtain high coulombic efficiency. Thus, the AB ratio and P/N mass ratio were fixed at 5 wt% and 2.0 for the subsequent cell tests for the effects of electrode thickness and density on the battery performance.

3.2 Effects of electrode thickness and density

It is essential to use thick and dense electrodes for high capacity batteries, provided that the applied current rate is moderate. However, at high current rates, too thick or too dense electrodes inevitably suffer from significant voltage loss due to slow ion transport in the liquid phase (so-called transport limitation). That is, increasing the electrode thickness and density above certain critical values may have negligible advantages in enhancing the cell discharge capacity. Thus, full cell tests were performed to find optimal

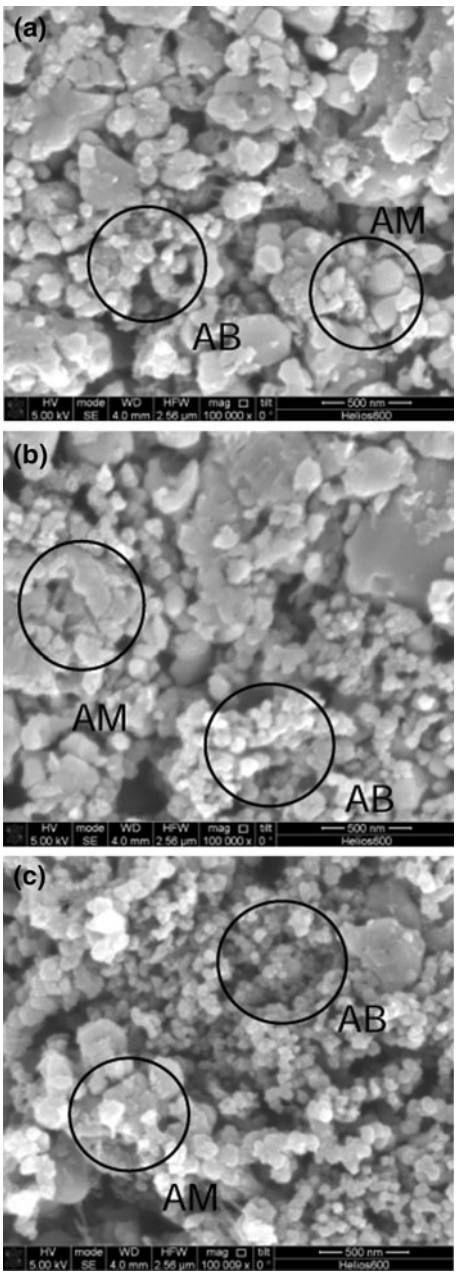

Fig. 2 The SEM images of the $LiFePO_4$ electrodes at the conductor ratio of **a** 2, **b** 8, and **c** 15 wt%

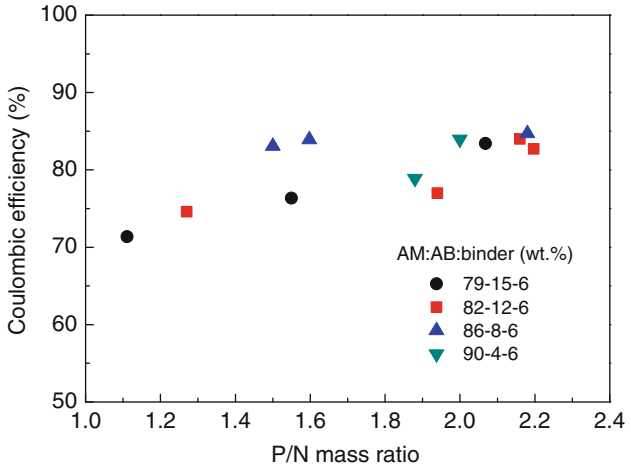

Fig. 3 The coulombic efficiency of the $LiFePO_4$/graphite full cells at the various P/N mass ratios and conductor ratios, measured at a constant current rate of 0.1 C

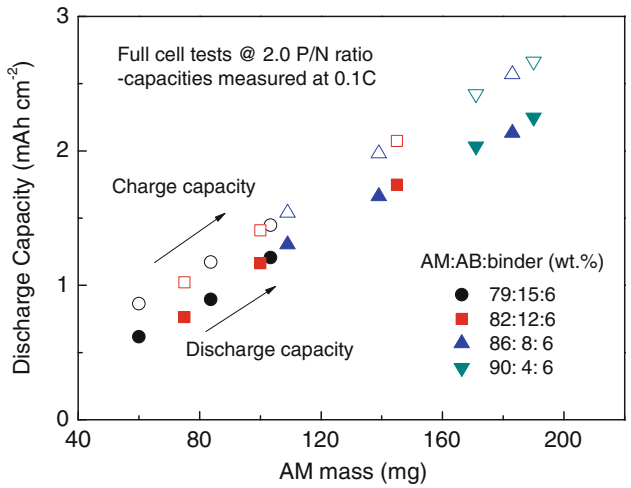

Fig. 4 The first-cycle charge and discharge capacities of the $LiFePO_4$/graphite full cells, measured at a constant current rate of 0.1 C

ranges for the electrode thickness and density to obtain high discharge capacity as well as high capacity efficiency. The electrode thickness was varied as 60–125 μm and the AM density of positive electrodes as 1.93–2.30 g cm^{-3}. The considered current rate was between 0.5 and 5 C.

Figure 5 shows the measured discharge capacity (mAh cm^{-2}) at various cathode thicknesses and current rates. The AM density of positive electrode was 2.05 g cm^{-3} for Fig. 5a and 2.15 g cm^{-3} for Fig. 5b. At low current rate (<1 C), the discharge capacity is found to increase rather proportionally to the electrode thickness or the mass of $LiFePO_4$ material. However, the voltage loss due to transport limitation causes additional capacity drop as the current rate increases, and this drop becomes significant as the electrode thickness increases. As shown in Fig. 5, thick electrodes suffer from severe capacity loss at high current rate (≥2 C), indicating too thick electrode should be avoided due to the transport limitations at high current rate.

At this moment, it should be noted that, at a fixed current rate, actual discharge current density is different for the test cells of different electrode thicknesses. Assuming the intrinsic charge capacity (measured at a very low current rate) is proportional to the electrode thickness, the test cell with 124 μm electrode thickness in Fig. 5a is subject to about two times larger discharge current density than that with 60 μm electrode thickness. Thus, increasing the

electrode thickness has double effects on the battery processes, assuming that the capacity of a $LiFePO_4$/graphite battery is fixed; first, the conduction and diffusion lengths in the electrodes are increased, and second, the current density and diffusion flux are increased. However, advantages of thicker electrodes are obvious; material and manufacturing cost and cell volume can be reduced because smaller cell area is required to make a battery of the same capacity.

In Fig. 5, the discharge capacities show relatively linear decrease with increase in the current rate, where the rate of capacity decrease is higher for thick electrodes. From Fig. 5, the slope of the capacity decrease below 2 C current rate was chosen as a meaningful index to evaluate the capacity loss due to the electrode thickness. That is, the measured discharge capacity, $Q(I)$, for the applied current rate, I, less than 2 C was fitted to the following correlation:

$$Q(I) = Q_0(L) - k(L) \cdot I, \quad (1)$$

where $Q_0(L)$ denotes the intrinsic discharge capacity at very low current rates and $k(L)$ denotes the rate of capacity loss (capacity loss coefficient) with respect to I.

Figure 6 illustrates $Q_0(L)$ and $k(L)$ measured from the cell tests with various electrode thicknesses and densities. As expected, the intrinsic discharge capacity, $Q_0(L)$, shows almost linear increase with respect to electrode thickness in Fig. 6a. Higher electrode density results in higher $Q_0(L)$ at the same electrode thickness and also higher slope of $Q_0(L)$. The capacity loss coefficient, $k(L)$, is shown in Fig. 6b, where $k(L)$ also increases when the electrode density or the electrode thickness is increased. Thus, thicker and dense electrodes improve the intrinsic discharge capacity but may result in higher capacity loss at higher current rates. In Fig. 6b, $k(L)$ is fitted to third-order polynomial curves with an inflection point at a certain electrode thickness, above which $k(L)$ starts to drastically increase. The inflection points were around 90 μm, which

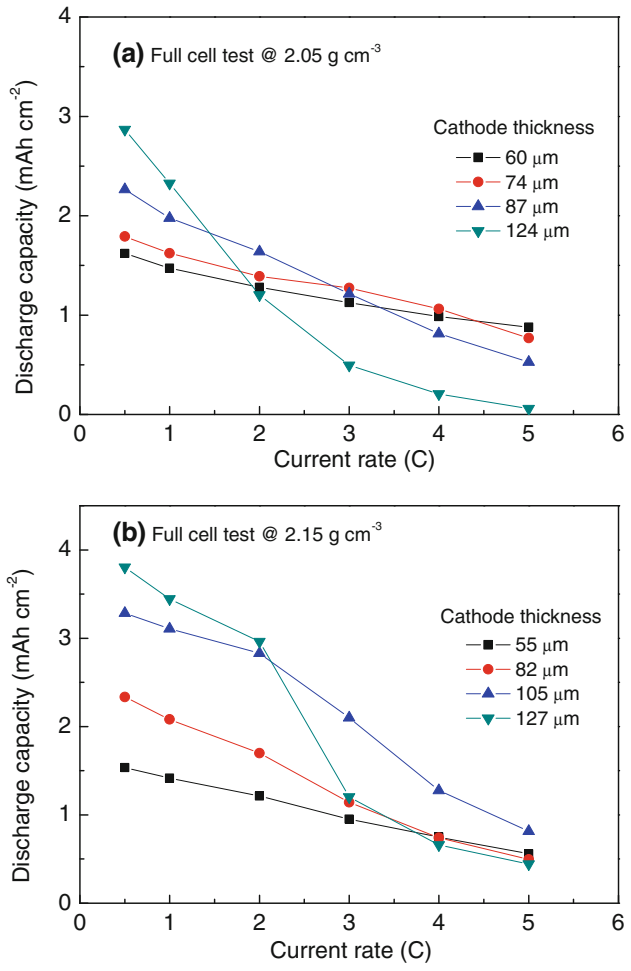

Fig. 5 The discharge capacity per unit area (mAh cm^{-2}) at various cathode thicknesses and current rates: **a** 2.05 g cm^{-3} and **b** 2.15 g cm^{-3}

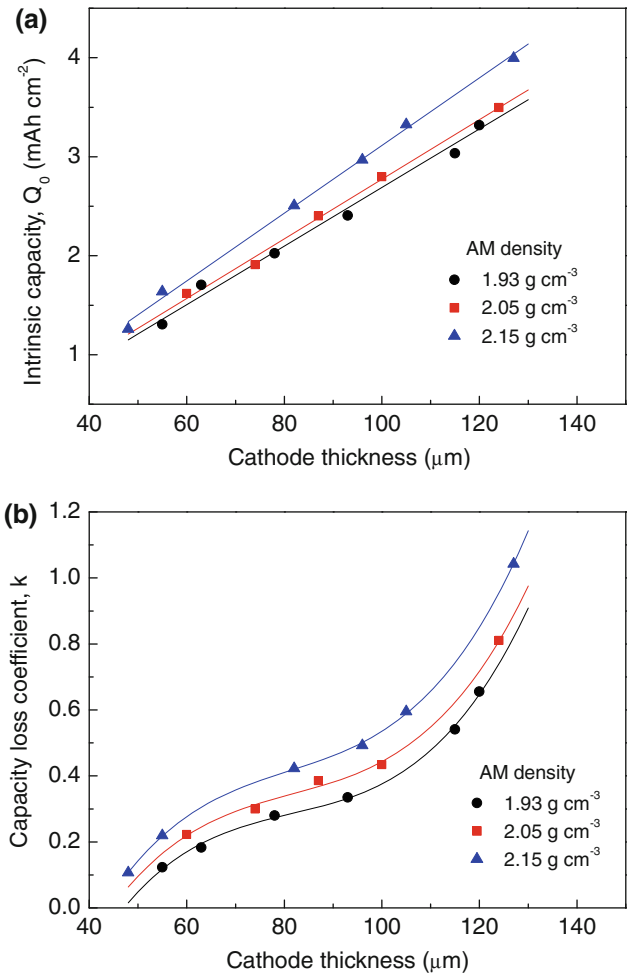

Fig. 6 The fitting results for discharge capacity degradation characteristics with various electrode thicknesses and densities: **a** intrinsic discharge capacity and **b** capacity loss coefficient

means that there is critical range of electrode thickness that leads to severe capacity loss.

Figure 7 shows the discharge capacity per unit area (mAh cm^{-2}) at various cathode thicknesses and current rates for the AM density of 2.15 and 2.30 g cm^{-3}. At low current rates (<1 C), the discharge capacity is found to increase rather proportional to the cathode thickness (the mass of the $LiFePO_4$ AM). At these low current rates, thick and dense electrodes can be designed to attain high discharge capacity without severe capacity drop due to the transport limitation. In Fig. 7, the discharge capacity for 120 μm electrode thickness can reach as high as 3.5 mAh cm^{-2} at 0.2 C current rate. Although obtained from the button cell tests, this discharge capacity is a very high value for $LiFePO_4$/graphite batteries. Thus, thick and dense electrodes can be successfully used in the applications that require high energy density with low current rate, such as energy storage system (ESS).

Figure 7 indicates that the electrode thickness of 120 μm can be used to obtain relatively high capacity of 2.5 mAh cm^{-2} at 1 C current rate. However, at higher current rates (≥2 C), the discharge capacity shows fast degradation as the electrode thickness exceeds 100 μm. This capacity loss is believed to be associated with the voltage loss due to the diffusion limitation. Thus, it is important to design the electrode thickness within the proper range to maintain high discharge capacity at higher current rates. Based on Fig. 7, the critical electrode thickness above which severe diffusion limitation at higher current rates (≥2 C) occurs can be estimated. For the AM density of 2.15 g cm^{-3} shown in Fig. 7a, b, the critical thickness is estimated to be about 120 μm for 1 C rate, about 100 μm at 2 C rate, and about 80 μm for higher rates (>2 C). However, in Fig. 7b for the AM density of 2.30 g cm^{-3}, the critical thickness is estimated to be below 70 μm at 2 C rate. This result clearly shows that using thick and dense electrodes to obtain high energy density can have negative impacts on the discharge capacity, especially at high current rates (≥2 C).

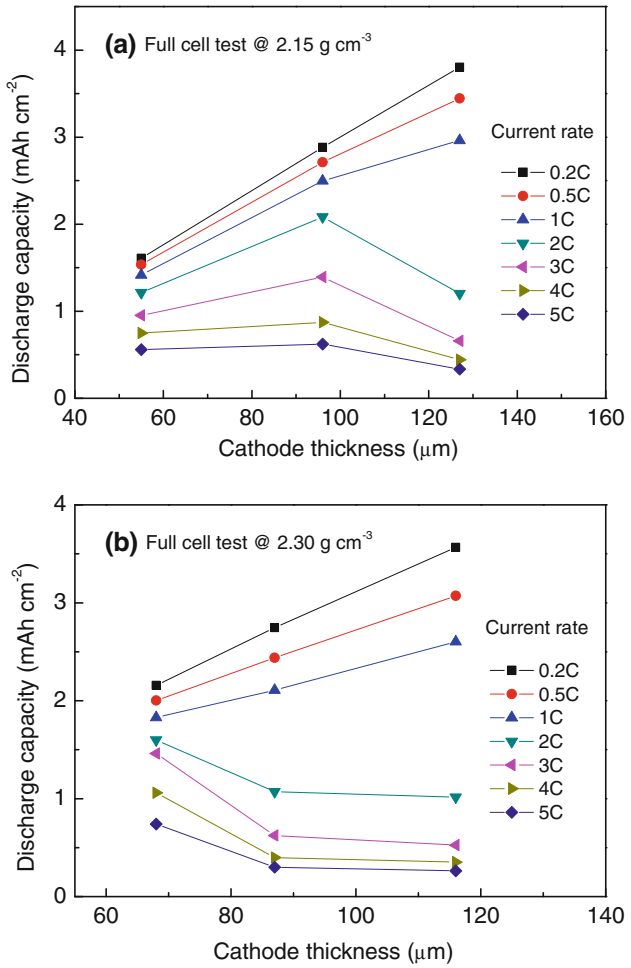

Fig. 7 The discharge capacity per unit area (mAh cm^{-2}) at various cathode thicknesses and current rates: **a** 2.15 g cm^{-3} and **b** 2.30 g cm^{-3}

A mathematical model was utilized to simulate the discharge behaviors of the experimental $LiFePO_4$/graphite cells and thus to investigate the mechanism of the observed performance loss in the thick and dense electrodes at high current rates. Figure 8 compares the experimental and numerical discharge curves at 1, 2, and 3 C rate with the AM density of 2.05 g cm^{-3} and electrode thickness of 100 μm. The validity of the present numerical simulation is insured by the relatively good agreement between the experimental and numerical results shown in Fig. 8. The physical parameters required for the numerical simulation are summarized in Tables 4 and 5. In Table 4, the solid-phase conductivity of the $LiFePO_4$ electrode was measured by a four-point probe technique, and the size of AM particles were determined from the SEM images. Several model parameters were chosen to best fit the experimental

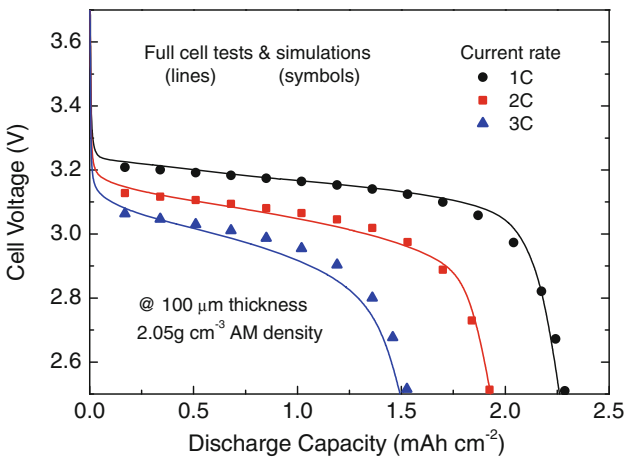

Fig. 8 The comparison between the measured (*lines*) and the predicted (*symbols*) discharge curves with 100 μm thickness and 2.05 g cm^{-3} AM density

discharge curves from the full cell tests with the $LiFePO_4$ electrodes as indicated in Table 4. The diffusion coefficient and the reaction rate constant were assumed to be constant.

Figure 9 shows the predicted concentration profiles of lithium ions at the end of discharge process (at the instance the discharge voltage reaches the cut-off voltage). The layer thickness was fixed as 25 μm for the separator and 100 μm for the cathode. For the anode, the layer thickness was set at 67.7 μm for the AM density of 2.05 and 71.2 μm for 2.15 g cm^{-3} (to obtain the same P/N ratio). In Fig. 9, the lithium ion concentration in the cathode decreases significantly as the distance from the separator increases, which is primarily due to the increased diffusion length for lithium ions and the intercalation of them into the AM particles. Figure 9 indicates the slope of the concentration drop in the cathode becomes steeper as the AM density or the applied discharge current rate increases. The ion transport in the electrolyte phase becomes more difficult in denser electrodes. Moreover, as the current rate increases, lithium ion cells suffer from more transport limitation due to the increased ionic and electronic flux through the electrodes.

Figure 10 shows the average SOC inside the cathode at the end of discharge process. Note that the average SOC denotes the degree of the lithium ion intercalation in the $LiFePO_4$ particles. That is, the SOC of 1 denotes all the intercalation sites in the AM are occupied by lithium ions. The simulation conditions are the same as used for Fig. 9. In Fig. 10, average SOC near the separator (at 0 μm cathode thickness) generally approaches to 0.9 as the discharge reaches the cut-off voltage of 2.5 V. However, average SOC near the current collector (at 100 μm electrode thickness) shows lower values, which is related with the lower lithium-ion concentrations near the current collector previously observed in Fig. 9. In Fig. 10, average

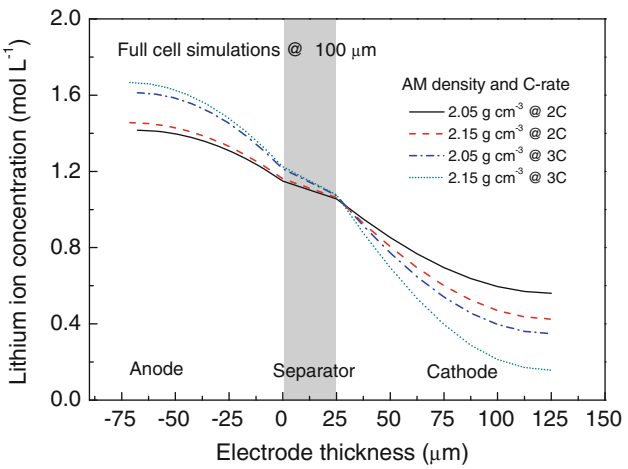

Fig. 9 The concentration profiles for lithium ion in electrolyte upon reaching the cut-off voltage (2.5 V) at various AM densities and current rates with 100 μm thickness

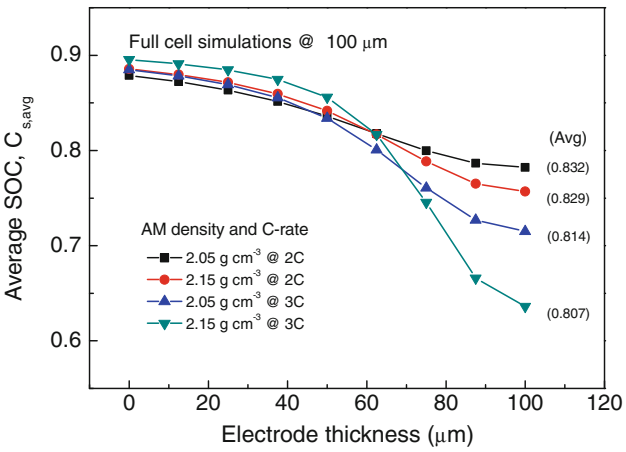

Fig. 10 The average SOC in cathode upon reaching the cut-off voltage (2.5 V) at various AM densities and current rates with 100 μm thickness

SOC near the separator increases slightly while that far from the separator decreases significantly, as the AM density or the current rate increases, and this leads to higher non-uniformity of average SOC inside cathode. The low SOC values much below 0.9 indicate the premature ending of discharge process caused by high voltage loss due to transport limitation in the electrolyte phase.

The SEM images (25,000×) of the $LiFePO_4$ electrodes are shown in Fig. 11, where the AM density was varied as 2.18, 2.23, and 2.35 g cm^{-3}. Figure 11 indicates that the electrode porosity decreases according to the degree of electrode compression. The performance loss due to the transport limitation in highly compressed electrodes can be clearly explained with these SEM images. When the AM density is 2.18 g cm^{-3}, larger pore spaces through which lithium ions can be easily transported can be observed in the SEM image. However, when the AM density approaches its practical limit of around 2.40 g cm^{-3}, such larger pore spaces seem to disappear, leaving many small pore spaces with highly tortuous paths. The ion transport is believed to be very difficult and thus the additional capacity loss due to the transport limitation is expected in such dense electrodes.

4 Conclusion

In this study, the optimal ranges for the electrode design parameters were investigated to achieve higher performance of the $LiFePO_4$/graphite batteries. The effects of the conductor ratio, electrode thickness, and AM density on the discharge capacity were studied, targeting their performance enhancement at high current rates. The effects of the conductor ratio were investigated first by conducting various cell tests with half and full cell structures. In addition, a four-point probe technique was used to measure the

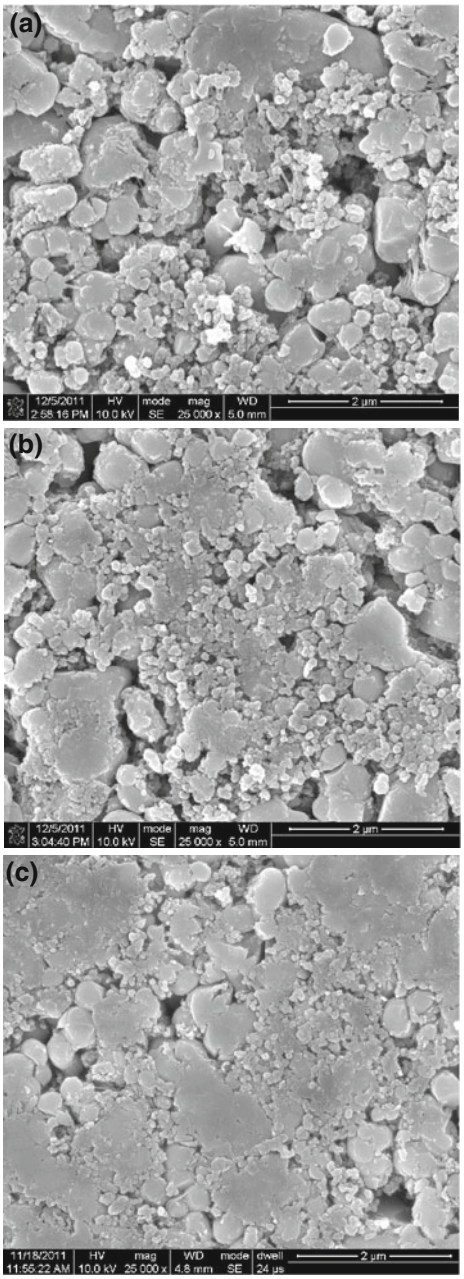

Fig. 11 The SEM images of the $LiFePO_4$ electrodes at various AM densities: **a** 2.18 g cm^{-3}, **b** 2.23 g cm^{-3} and **c** 2.35 g cm^{-3}

electrode conductivity, and the SEM imaging was used to inspect the microstructural changes with conductor ratio. Based on the results, the conductor ratio of around 5 wt% and the P/N mass ratio of about 2.0 were chosen as the suitable ranges for high electrical conductivity as well as high volumetric energy density.

Then, the effects of the electrode thickness and AM density on the performance were investigated at a fixed conductor ratio of 5 wt%. At low current rates, thick and dense electrodes were found to beneficial to attain high discharge capacity. Under 1 C rate, $LiFePO_4$ electrodes as thick as 120 μm could be used to achieve high capacity (>2.5 mAh cm^{-2} at 1 C rate). However, discharge capacity with thick electrodes (>100 μm) starts to rapidly degrade at high current rates. For AM density ratio of 2.15 g cm^{-3}, the critical thickness was estimated to be about 80–100 μm at the current rate higher than 2 C. However, for AM density ratio of 2.30 g cm^{-3}, this critical thickness was reduced to be below 70 μm at 2 C rate. Therefore, the electrodes for high current applications should be designed to have proper thickness and AM density to avoid additional capacity loss associated with the transport limitation.

Numerical model simulation also proved that ion transport in the electrolyte phase becomes more difficult in dense electrodes. The voltage loss due to this transport limitation was found to make the discharge voltage to reach the cut-off voltage before full utilization of the AM particles, causing premature ending of discharge process. The SEM images for compressed electrodes were also inspected, which pointed out that high electrode compression to obtain high energy density may cause severe transport loss by reducing the effective diffusivity and conductivity in electrolyte phase.

Acknowlegments This work was supported by the Energy Efficiency & Resources program of the Korea Institute of Energy Technology Evaluation and Planning (KETEP) grant funded by the Korea government Ministry of Knowledge Economy (20092010100 03B-11-3-020 and 20102010100090-11-2-200).

References

1. Huang H, Yin SC, Nazar LF (2001) Electrochem Solid State Lett 4:A170
2. Chen Z, Dahn JR (2002) J Electrochem Soc 149:A1184
3. Prosini PP, Zane D, Pasquali M (2001) Electrochim Acta 46:3517
4. Wilcox JD, Doeff MM, Marcinek M, Kostecki R (2007) J Electrochem Soc 154:A389
5. Chung SY, Bloking JT, Chiang YM (2002) Nat Mater 1:123
6. Wang D, Li H, Shi S, Huang X, Chen L (2005) Electrochim Acta 50:2955
7. Shi S, Liu L, Ouyang C, Wang DS, Wang Z, Chen L, Huang X (2003) Phys Rev B 68:195108
8. Sides CR, Croce F, Young VY, Martion CR, Scrosati B (2005) Electrochem Solid State Lett 8:A484
9. Kim DH, Kim J (2006) Electrochem Solid State Lett 9:A439
10. Delacourt C, Poizot P, Levasseur S, Masquelier C (2006) Electrochem Solid State Lett 9:A352
11. Jiao F, Hill AH, Harrison A, Berko A, Chadwick A, Bruce PG (2008) J Am Chem Soc 130:5262
12. Dominko R, Bele M, Goupil JM, Gaberscek M, Hanzel D, Arcon I, Jamnik J (2007) Chem Mater 19:2960
13. Chen YH, Wang CW, Zhang X, Sastry AM (2010) J Power Sour 195:2851
14. Fongy C, Gaillot AC, Jouanneau S, Guyomard D, Lestriez B (2010) J Electrochem Soc 157:A885
15. Gaberscek M (2009) J Power Sour 189:22
16. Doyle M, Fuller TF, Newman J (1993) J Electrochem Soc 140:1526

17. Fuller TF, Doyle M, Newman J (1994) J Electrochem Soc 141:1
18. Fuller TF, Doyle M, Newman J (1994) J Electrochem Soc 141:982
19. Doyle M, Newman J (1996) J Electrochem Soc 143:1890
20. Srinivasan V, Newman J (2004) J Electrochem Soc 151:A1517
21. Srinivasan V, Newman J (2004) J Electrochem Soc 151:A1530
22. Singh GK, Ceder G, Bazant MZ (2008) Electrochim Acta 53:7599
23. Tang M, Carter WC, Chiang YM (2010) Annu Rev Mater Res 40:501
24. Tang M, Belak JF, Dorr MR (2011) J Phys Chem C 115:4922
25. Zhang SS, Jow TR (2002) J Power Sour 109:72
26. Hong JK, Lee JH, Oh SM (2002) J Power Sour 111:90